

Quantitative Analysis of Sodium Metal Deposition and Interphase in Na Metal Batteries

Baharak Sayahpour¹, Weikang Li², Shuang Bai¹, Bingyu Lu², Bing Han², Yu-Ting Chen¹, Grayson Deysher¹, Saurabh Parab¹, Phillip Ridley², Ganesh Raghavendran², Long Hoang Bao Nguyen², Minghao Zhang^{2,*}, Ying Shirley Meng^{2,3,*}

¹Materials Science and Engineering program, University of California San Diego, CA 92093, USA

²Department of NanoEngineering, University of California San Diego, CA 92093, USA

³Pritzker School of Molecular Engineering, University of Chicago, Chicago, IL 60637, USA

*Corresponding authors, miz016@eng.ucsd.edu, shirleymeng@uchicago.edu

Keywords: Sodium Deposition, Sodium Metal Anode, Solid Electrolyte Interphases, Cryogenic Electron Microscopy, High-rate Sodium Metal Battery.

Table of Content

Section S1. Properties of Materials.

Section S2. Titration Gas Chromatography (TGC) Method

Section S3. Uniaxial Pressure Setup

Section S4. Cryogenic Focused Ion Beam Scanning Electron Microscopy (Cryo-FIB-SEM)

Section S5. Electrochemical Impedance Spectroscopy (EIS)

Section S6. X-ray Photoelectron Spectroscopy (XPS)

Section S7. Cryogenic Scanning Electron Microscopy (cryo-STEM) and Cryogenic Electron Energy Loss Spectroscopy (cryo-EELS)

Section S8. Electrochemical Performance – Ether-based Electrolyte

Section S9. Self-Discharge

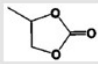
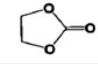
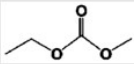
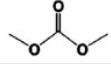
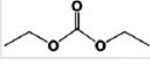

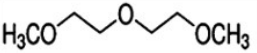
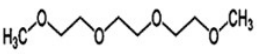
Section S10. Electrochemical Performance – Carbonate-based Electrolyte

Section S1. Properties of Materials

Table S1. The physical, mechanical, and electrochemical properties of sodium in comparison with lithium.

Physical Properties						Mechanical Properties		Electrochemical Properties		
Atomic Weight (g/mol)	Atomic Radius (Å)	Ionic Radius (Å)	Molar Volume (cm ³ /mol)	Melting Point (K)	Heat of Vaporization (kJ/mol)	Bulk Modulus (GPa)	Brinell Hardness (MPa)	Voltage vs. SHE (V)	1 st ionization energy (kJ/mol)	
Na	23	1.86	1.02	23.75	371	97	6.3	0.69	-2.7	495.8
Li	6.9	1.52	0.76	12.97	454	136	11	5	-3.0	520.2

Table S2. The physical properties of the common carbonate- and ether- based solvents. Abbreviations: PC, propylene carbonate; EC, ethylene carbonate; EMC, ethyl methyl carbonate; DMC, dimethyl carbonate; DEC, diethyl carbonate; DME, dimethoxyethane; DEGDME, diglyme; TEGDME, tetraethylene glycol dimethyl ether.

	Chemical Structure	Viscosity (η) [cP at 25°C]	Dielectric Constant (ϵ at 25°C)	Melting Point (T_m) [°C]	Boiling Point (T_b) [°C]	Flash Point (T_f) [°C]
Carbonate-based	PC 	2.53	64.92	-48.8	242	132
	EC 	1.9	89.78	36.4	248	160
	EMC 	0.65	2.958	-53	110	
	DMC 	0.59	3.107	4.6	91	18
	DEC 	0.75	2.805	-74.3	126	31
Ether-based	DME 	0.46	7.18	-58	84	0
	DEGDME 	1.06	7.4	-61	162	57
	TEGDME 	3.39	7.53	-46	216	111

Section S2. Titration Gas Chromatography (TGC) Method

It was previously shown in our group that the trapped metallic lithium known as the dead lithium is the main source of capacity loss in the lithium plating and stripping, leading to the loss of coulombic efficiency.^{1,2} In that study, TGC method was developed as a quantitative tool to precisely measure the metallic lithium content by detecting the generated hydrogen (H₂) gas from the reaction of the metallic lithium with water (H₂O) through this fellow reaction:



In this study, we extended this unique method for sodium metal to precisely quantify the sodium loss in different carbonate- and ether- based electrolytes.

One major difference in the case of sodium metal compared to lithium metal is the use of aluminum (Al) as the current collector instead of copper (Cu). Al is not reactive with sodium at the reduced potentials despite the case of lithium and is widely used as the current collector in sodium ion batteries due to its higher abundance (abundance in earth's crust: 8.23% for Al and 0.0068% for Cu)³ and lower cost than Cu. However, Al cannot be used in TGC method with water as the solvent because of the formation of the hydrofluoric (HF) acid as a side reaction of water with NaPF₆ salt or possible SEI components, such as sodium fluoride (NaF), that further can generate H₂ gas in reaction with Al.⁴ Because of this matter, we utilized ethanol (EtOH) as the solvent in TGC study for the case of sodium metal.

First, in order to investigate the impact of solvents and salts on the ICE of Na metal anode, Na plating and stripping was performed with different solvent and salt combinations. The case studies of solvents are listed as 1M NaPF₆ in PC, 1M NaPF₆ in EC:PC (1:1), 1M NaPF₆ in PC with 2wt% FEC, 1M NaPF₆ in EC:PC (1:1) with 2wt% FEC, 1M NaPF₆ in EC:PC:DMC (45:45:10), 1M NaPF₆ in EC:DMC (1:1), 1M NaPF₆ in DME, 1M NaPF₆ in DEGDME, and 1M NaPF₆ in TEGDME, and the case studies of salts are listed as 1M NaPF₆, 1M NaBF₄, and 1M NaFSI in EC:DMC (1:1) and in DME. The first cycle voltage profiles and coulombic efficiencies are shown in **Figure S1** in SI file.

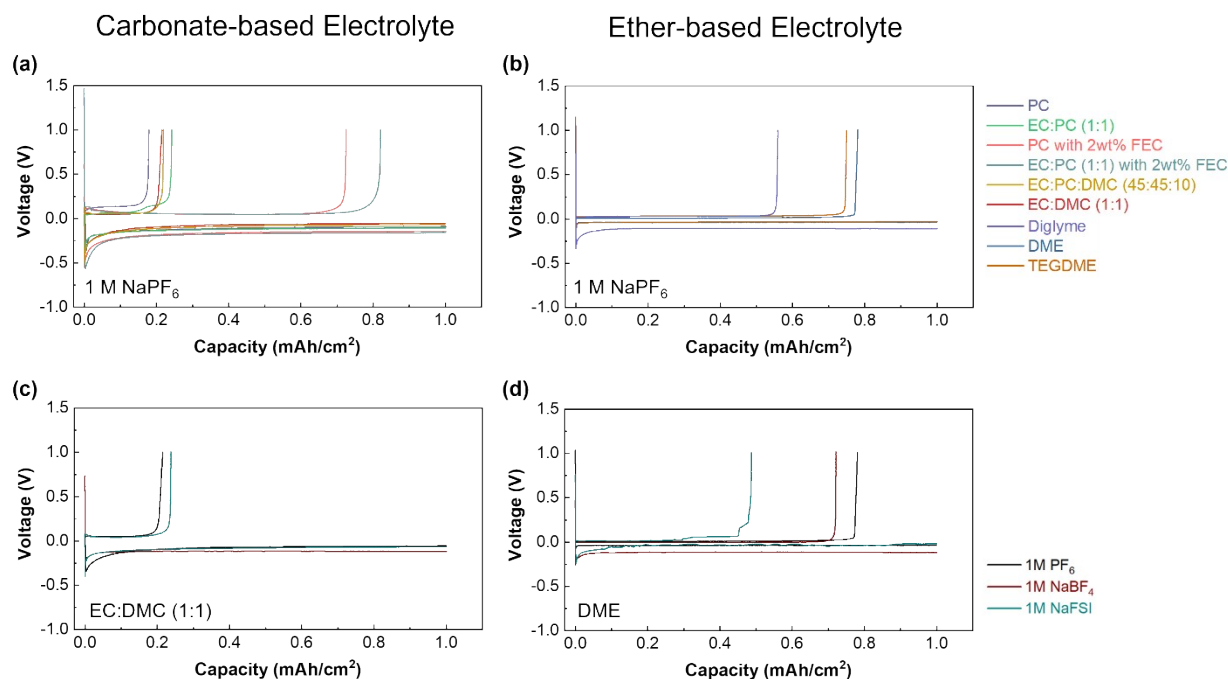


Figure S1. The 1st cycle plating and stripping voltage profile of Na||Al coin-cells using (a) 1 M NaPF₆ in carbonate-based solvents, (b) 1 M NaPF₆ in ether-based solvents. (c) 1 M different salts in carbonate-based solvent; EC:DMC (1:1), and (d) 1 M different salts in ether-based solvent; DME. The Na was plating at 0.5 mA/cm² for 1 mAh/cm² followed by stripping to 1 V at 0.5 mA/cm² on the Al foil.

TGC was performed using a Shimadzu GC instrument equipped with a BID detector and ultra-high purity Helium (99.999%) as the carrier gas. The samples were prepared in an Ar-filled glovebox with < 0.1 ppm H₂O level. Each sample was immediately transferred to a glass flask after disassembling and sealed using a septum under Ar. 0.5 mL of ethanol was injected into the container to fully react with metallic sodium. After reaction completion, a 30 μ L gas sample was taken from the container using a gastight Hamilton syringe and immediately injected into the GC. The amount of metallic sodium was quantified based on the amount of detected H₂ gas by the GC.

The TGC technique was performed on the stripped Al current collector after the first cycle of the sodium plating at the rate 0.5 mA/cm² for the total capacity of 1 mAh/cm² and followed by the sodium stripping to cut-off voltage of 1 V at the same rate of 0.5 mA/cm².

Quantification of capacity usage and capacity loss using TGC method is shown in **Figure S2**. SEI formation is quantitatively shown as the main component of the capacity loss in the first cycle. Analysis of capacity usage (reversible Na, unreacted metallic Na⁰, and SEI Na⁺) and capacity loss (unreacted metallic Na⁰ and SEI Na⁺) are shown for the 1 M NaPF₆ in different solvents; carbonate-based and ether-based, and for the 1 M of the different salts in carbonate-based solvent; EC:DMC (1:1 vol%) and in ether-based solvent; DME.

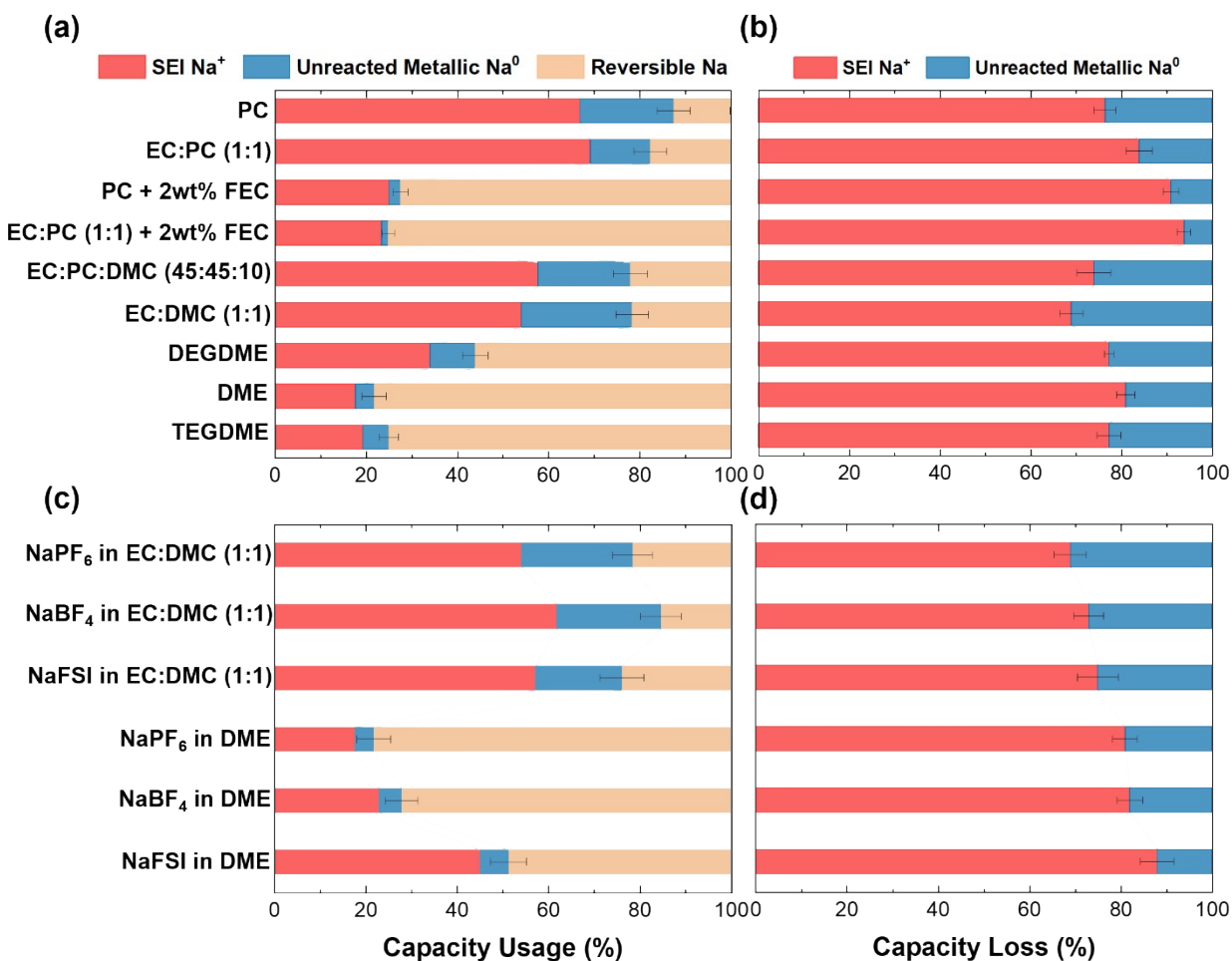


Figure S2. Quantification of capacity usage and capacity loss using TGC method. SEI formation is quantitatively shown as the main component of the capacity loss in the first cycle. Analysis of capacity usage (reversible Na⁰, unreacted metallic Na⁰, and SEI Na⁺) and capacity loss (unreacted metallic Na⁰ and SEI Na⁺) are shown **(a-b)** using 1 M NaPF₆ in different solvents; carbonate-based and ether-based, and **(c-d)** using 1 M of the different salts in carbonate-based solvent; EC:DMC (1:1 vol%) and in ether-based solvent; DME. The Na||Al cells were plating at 0.5 mA/cm² for 1 mAh/cm² followed by stripping to 1V at 0.5 mA/cm².

The TGC results revealed that there is a correlation between unreacted metallic sodium and the first cycle coulombic efficiency: the more unreacted metallic sodium (Na^0) the lower the first cycle coulombic efficiency.

It should be noted that PC does not work with celgard due to its wettability issue⁵ and therefore other separators such as glass fiber are required that raise some challenges such as: higher electrolyte consumption, lower total energy density, and the impossibility of surface characterization and visualization. The mixture of EC:DMC as the solvent is one of the most attractive and commonly used solvents in SIBs due to beneficiary from the combination of EC with the highest dielectric constant (89.78 at 25°C) and DMC with the lowest viscosity (0.59 cP at 25°C).^{6,7} The cosolvent systems show exclusive enhancements in ion conductivity, viscosity, and electrochemical stability of the electrolyte.^{8,9}

Furthermore, a set of controlled experiments were performed on the available commercial sodium powder standards and salts to evaluate the possible formation of H_2 gas from the other sources. The results of these controlled tests are shown in **Figure S3**.

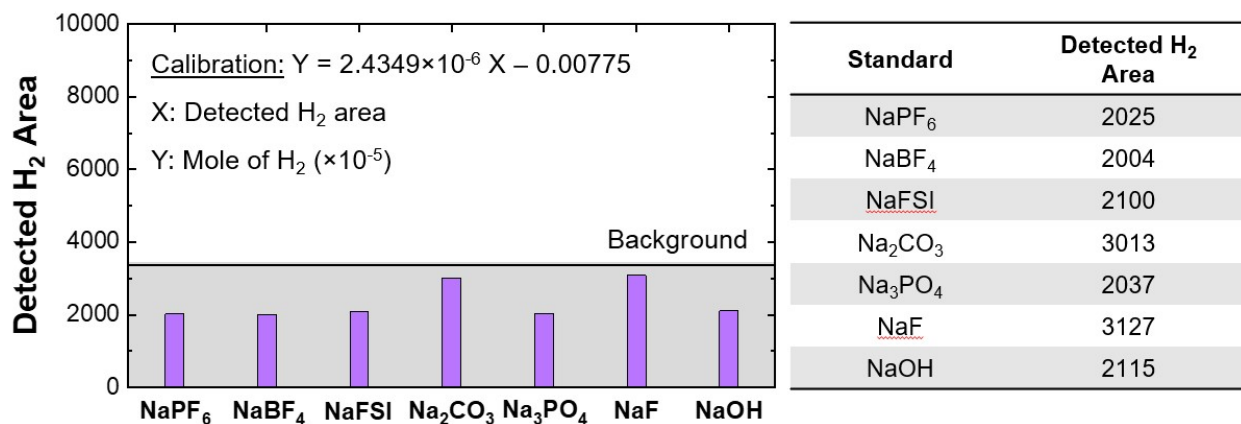


Figure S3. The controlled TGC experiment on standard commercial powders showed no hydrogen generation. This test was performed using ethanol as the solvent.

Section S3. Uniaxial Pressure Setup

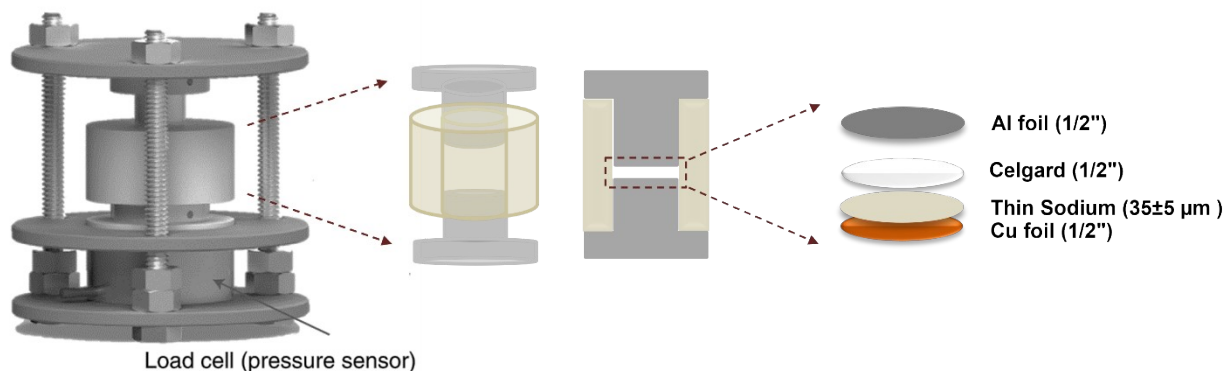


Figure S4. The schematic of the pressure setup and the cell components used in this study. The uniaxial pressure was controlled using the load cell. This setup was developed in our group.^{10,11}

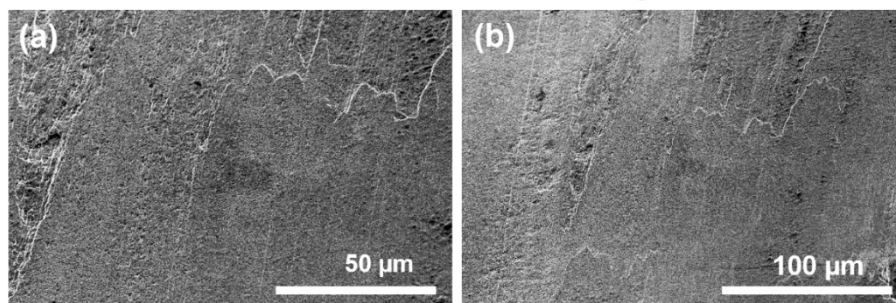
Section S4. Cryogenic Focused Ion Beam Scanning Electron Microscopy (Cryo-FIB-SEM)

The FIB-SEM was conducted on the FEI Scios Dual-beam microscopy; the discharged cells were disassembled in the Ar-filled glovebox after cycling. The samples were transferred to the FIB chamber via quick loader without any exposure to air. The electron beam operating voltage was 5 kV, and the stage was cooled with liquid nitrogen to -180 °C or below. Sample cross-sections were exposed using a 1 nA ion beam current and cleaned at 0.1 nA.

Figure S5 shows the top and cross-sectional imaging on commercial sodium metal bulk at room-temperature condition. Yet there is clear damage on the sodium surface at top-view imaging before the ion milling (**Figure S5a-b**), the sodium reacts more vigorously after the ion exposure as can be seen in **Figure S5c-d** on top and surrounding areas of the ion milling.

On the other hand, the smooth surfaces of sodium metal in the top and cross-sectional imaging before and after ion milling, shown in **Figure S6**, indicate the necessity of the cryogenic condition for reliable imaging of the sodium metal.

Top view – Before Milling



Top and cross-sectional view – After Milling

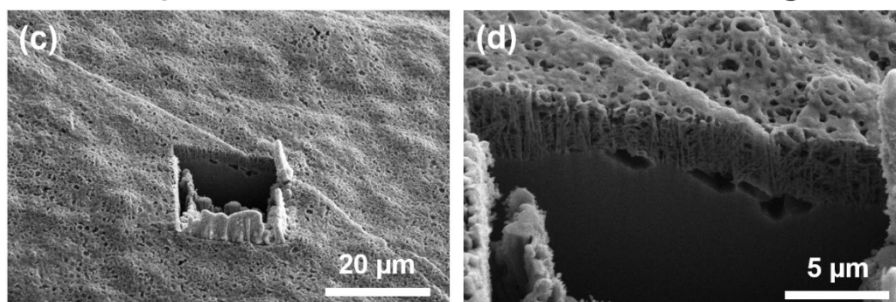
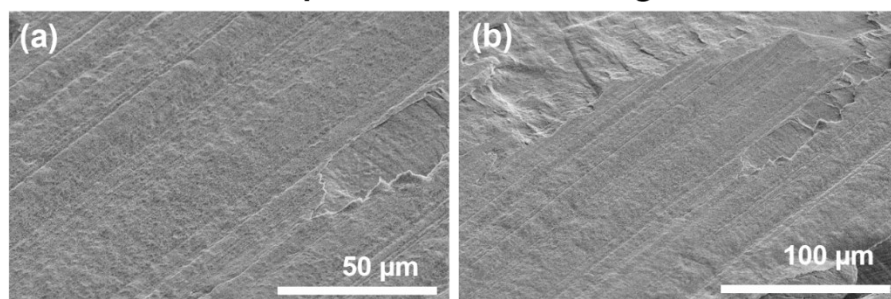


Figure S5. The surface of sodium is unstable at room temperature. The images at room temperature are shown for (a-b) top-view before milling, (c) top-view after milling, and (d) cross-sectional view after milling. The sample is freshly cut commercial sodium metal.

Top view – Before Milling



Top and cross-sectional view – After Milling

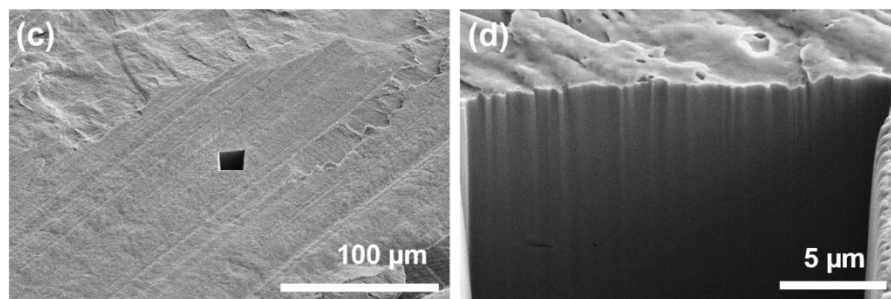


Figure S6. The surface of sodium is stable at cryogenic temperature. The images at cryogenic temperature are shown for (a-b) top-view before milling, (c) top-view after milling, and (d) cross-sectional view after milling. The sample is freshly cut commercial sodium metal.

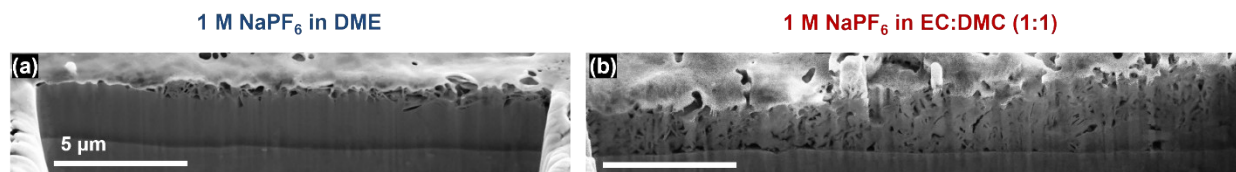


Figure S7. Cross-sectional cryogenic FIB-SEM images of the plated sodium at 10 kPa uniaxial pressures **(a)** in 1M NaPF₆ in DME electrolyte and **(b)** in 1M NaPF₆ in EC:DMC (1:1) electrolyte. The sodium was plated at 0.5 mA/cm² for 0.1 mAh/cm² on Al foil.

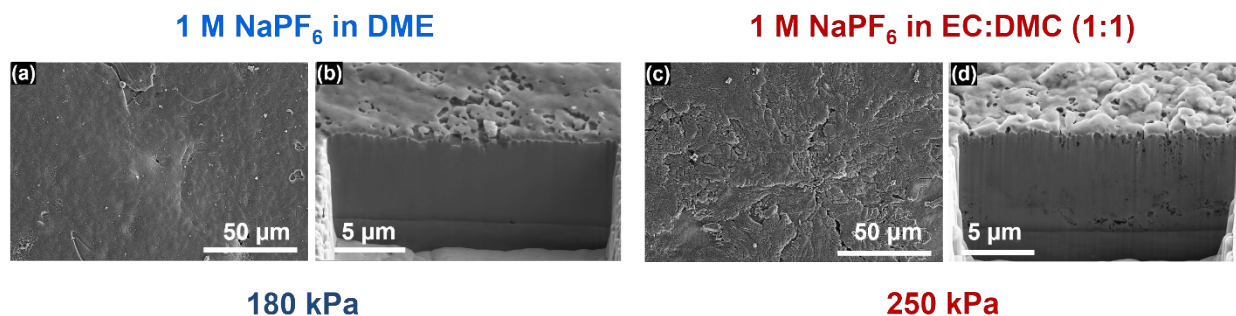


Figure S8. Top-view and cross-sectional cryogenic FIB-SEM images of plated sodium surface **(a-b)** in 1M NaPF₆ in DME electrolyte under 180 kPa uniaxial pressure and **(c-d)** in 1M NaPF₆ in EC:DMC (1:1) electrolyte under 250 kPa uniaxial pressure. The sodium was plated at 0.5 mA/cm² for 1 mAh/cm² on Al foil. These images are corresponding to Figure 1c and 1d.

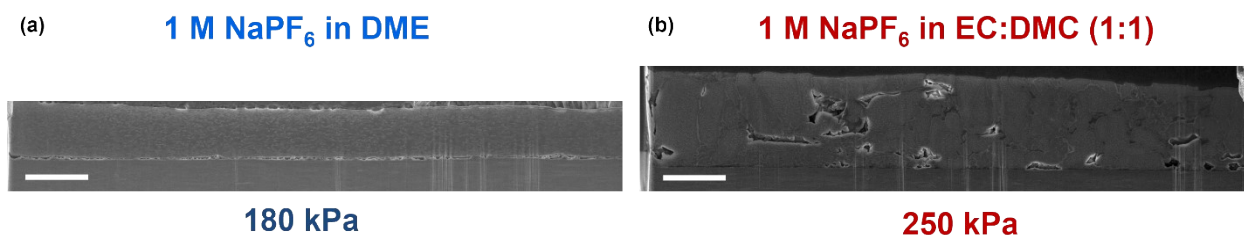


Figure S9. Cross-sectional plasma FIB-SEM images of plated sodium **(a)** in 1M NaPF₆ in DME electrolyte under 180 kPa uniaxial pressure and **(b)** in 1M NaPF₆ in EC:DMC (1:1) electrolyte under 250 kPa uniaxial pressure. The sodium was plated at 0.5 mA/cm² for 1 mAh/cm² on Al foil. The images are acquired under 5kV voltage and 0.2 nA current using a TLD detector. The scale bars are 10 μm.

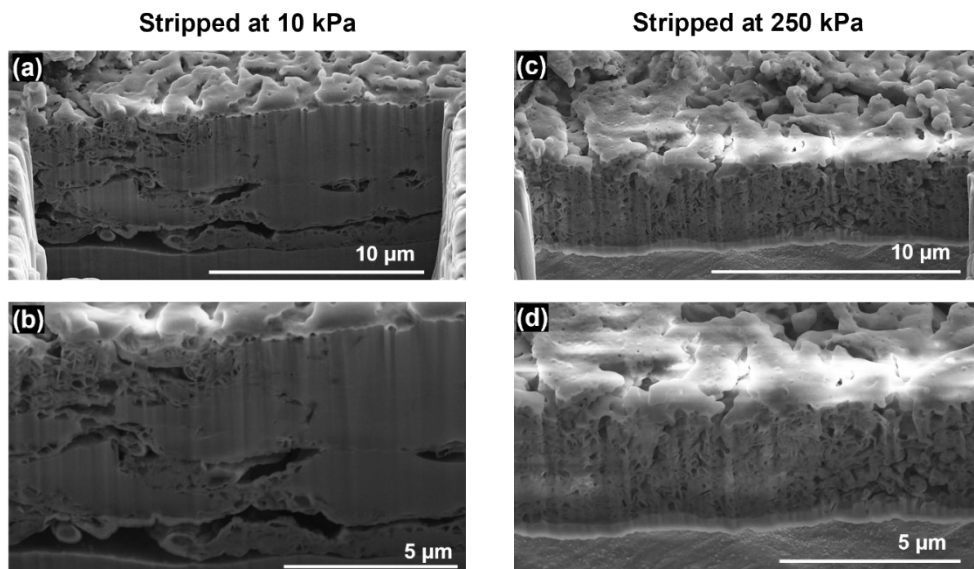


Figure S10. The cross-sectional cryogenic FIB-SEM images of the half-stripped sodium in 1M NaPF₆ in EC:DMC (1:1) at **(a-b)** 10 kPa and **(c-d)** 250 kPa. The sodium was plated at 0.5 mA/cm² for 1 mAh/cm² on Al foil at 250 kPa uniaxial pressure and stripped at 0.5 mA/cm².

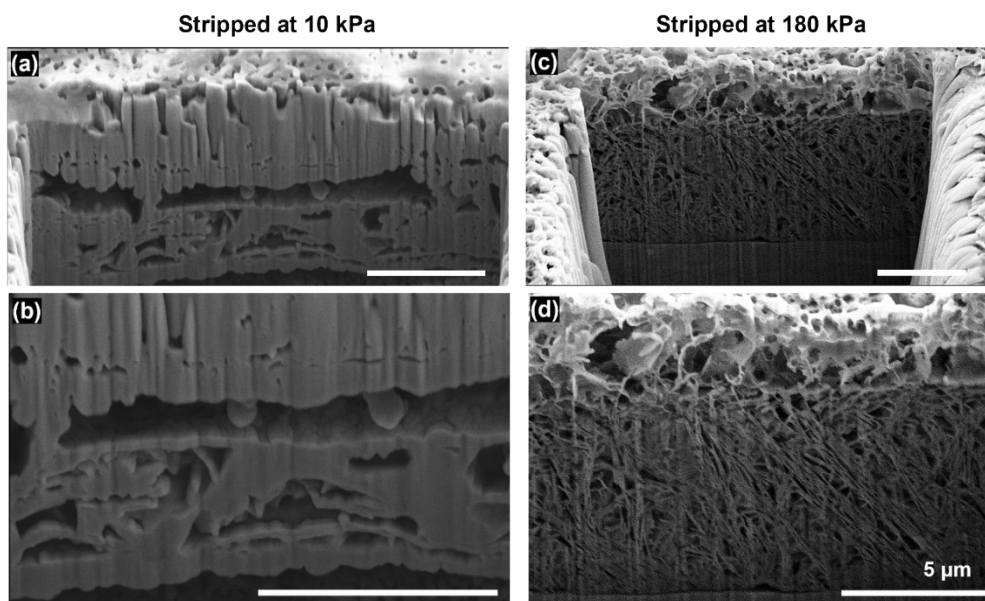


Figure S11. The cross-sectional cryogenic FIB-SEM images of the half-stripped sodium in 1M NaPF₆ in DME at **(a-b)** 10 kPa and **(c-d)** 180 kPa. The sodium was plated at 0.5 mA/cm² for 1 mAh/cm² on Al foil at 180 kPa uniaxial pressure and stripped at 0.5 mA/cm².

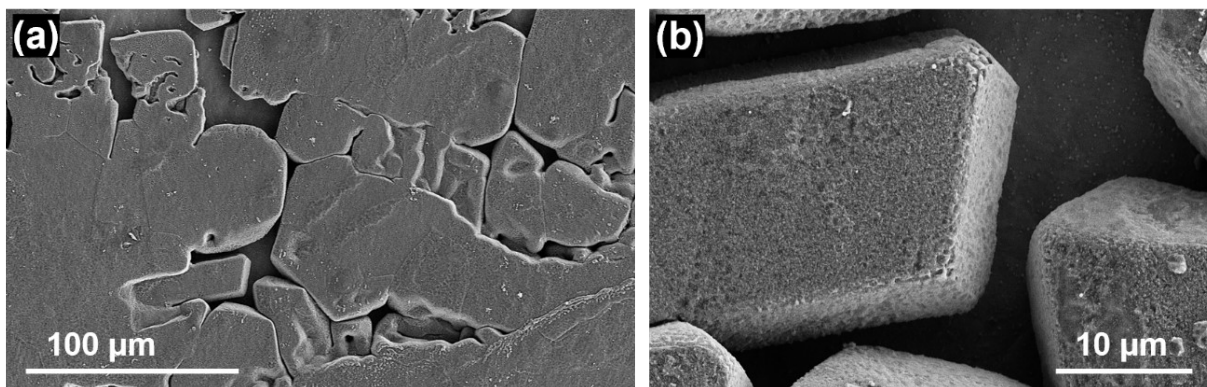


Figure S12. Top-view cryogenic FIB-SEM images of plated sodium in 1M NaPF₆ in DME electrolyte under 10 kPa. The sodium was plated at 0.5 mA/cm² for 1 mAh/cm² on Al foil at 10 kPa uniaxial pressure.

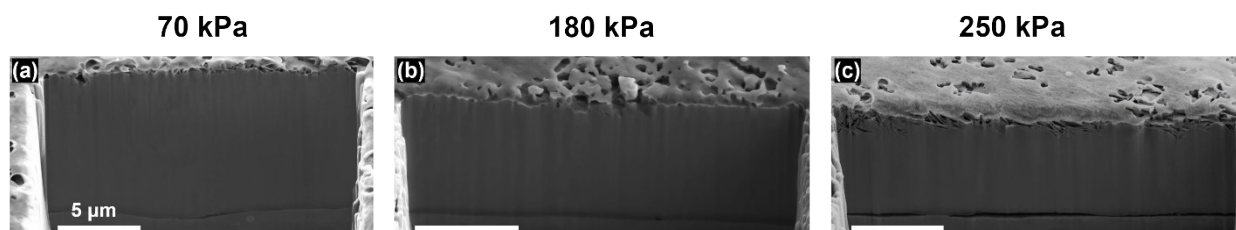


Figure S13. Cross-sectional cryogenic FIB-SEM images of the plated sodium in 1M NaPF₆ in DME electrolyte under the uniaxial pressures of (a) 70 kPa, (b) 180 kPa, (c) 250 kPa. The sodium was plated on Al foil at 0.5 mA/cm² for 0.1 mAh/cm² in (a) and for 1 mAh/cm² in (b-e). The scale bars are 5 μm.

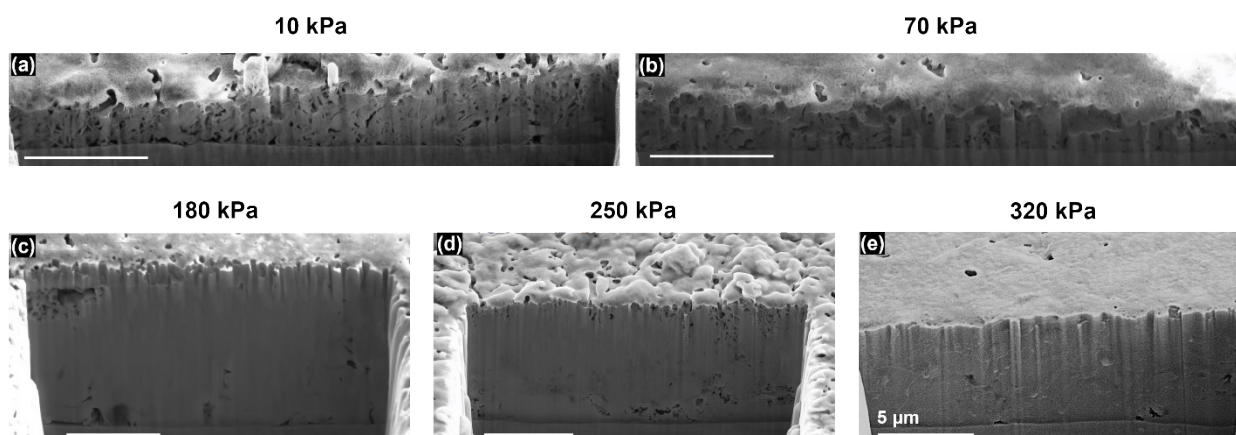
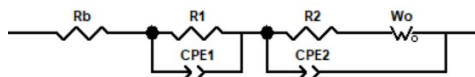


Figure S14. Cross-sectional cryogenic FIB-SEM images of the plated sodium in 1M NaPF₆ in EC:DMC (1:1) electrolyte under the uniaxial pressures of (a) 10 kPa, (b) 70 kPa, (c) 180 kPa, (d) 250 kPa, and (e) 320 kPa. The sodium was plated on Al foil at 0.5 mA/cm² for 0.1 mAh/cm² in (a-b) and for 1 mAh/cm² in (c-e). The scale bars are 5 μm.

Section S5. Electrochemical Impedance Spectroscopy (EIS)

EIS was performed with an applied AC potential of 10 mV in the frequency range of 1 MHz to 0.01 Hz, using a Solartron 1260 impedance analyzer. The EIS measurements for each case were performed on the same cell setup in the three steps: as-assembled (bare), after the first plating, and after the first stripping. The following equivalent circuit was used to analyze the data:



R_b reflects the overall resistance of electrolyte and current collectors, R_1 and R_2 reflect the charge transfer resistance ($\text{Na}^0 \rightarrow \text{Na}^+$) and the interfacial resistance from the ion migration through the SEI layer, CPE reflects their double layer capacitance, and W_0 reflects the Warburg impedance. The Nyquist plots for the as assembled, after the first plating, and after the first stripping steps at 10 kPa and optimum pressures are shown in **Figure S15**.

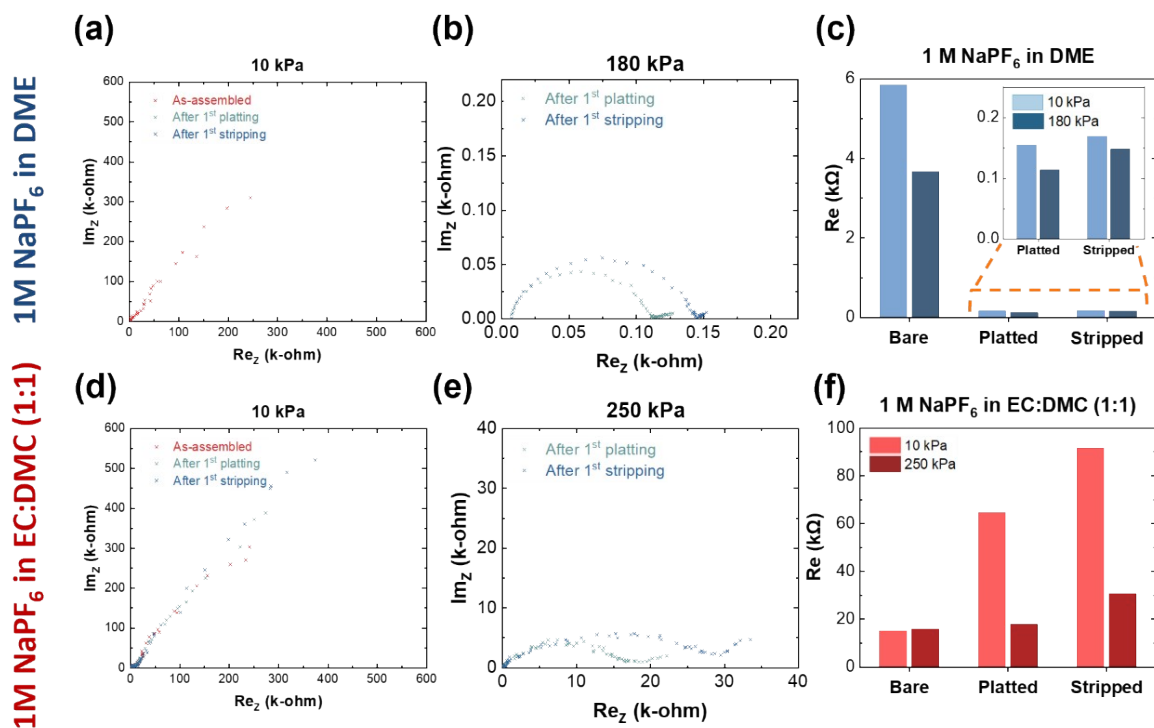


Figure S15. EIS measurement of Na||Al cells using both electrolytes at minimum and optimum pressures at three stages. The data for DME is shown for (a) 10 kPa and (b) 180 kPa, and (c) the overall comparison (R_1+R_2). The data for EC:DMC is shown for (d) 10 kPa and (e) 250 kPa, and (f) the overall comparison (R_1+R_2).

Section S6. X-ray Photoelectron Spectroscopy (XPS)

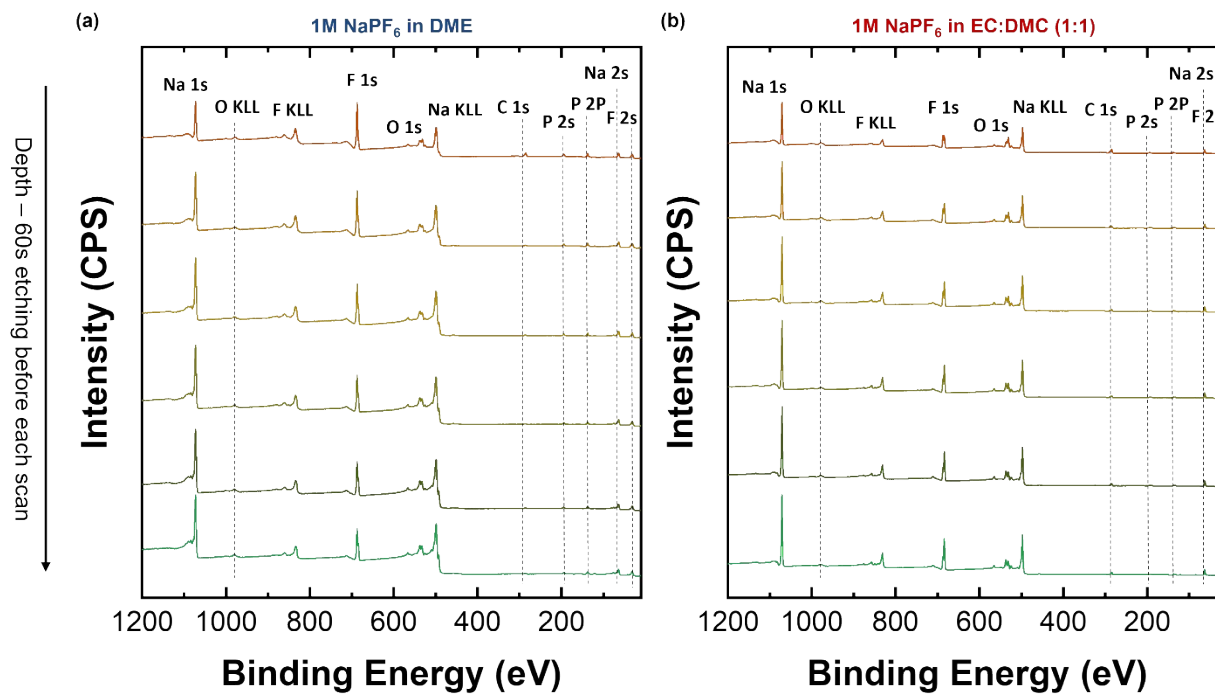


Figure S16. XPS spectra at different depth of etching on the SEI in the binding energy range of 1200-10 eV. The spectra show the presence of Na, C, F, O, and P bonding and there is no impurity from any other elements. The data is shown for (a) 1M NaPF₆ in DME electrolyte and (b) 1M NaPF₆ in EC:DMC (1:1) electrolyte. The samples were prepared under optimal pressures.

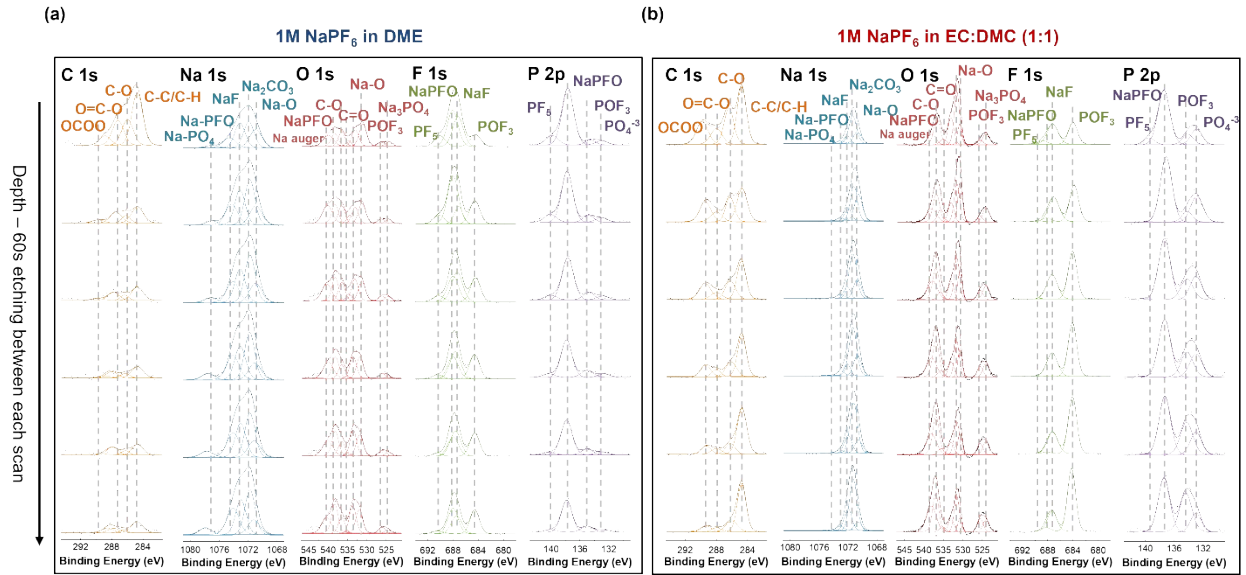


Figure S17. The surface characterization of SEI layer using the depth profiling XPS on the stripped sodium sample in C 1s, Na 1s, O 1s, F 1s, and P 2p regions. The data through the depth of etching is presented for the case of (a) 1M NaPF₆ in DME, and (b) 1M NaPF₆ in EC:DMC (1:1). The samples were prepared under optimal pressures.

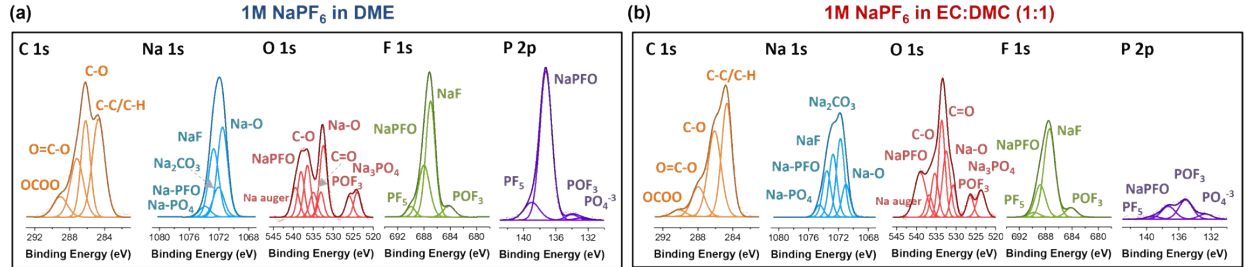


Figure S18. The X-ray photoelectron spectroscopy (XPS) depth profiling spectra in C 1s, Na 1s, O 1s, F 1s, and P 2p core levels for (a) 1M NaPF₆ in DME and (b) 1M NaPF₆ in EC:DMC (1:1). The samples were prepared under 10 kPa uniaxial pressure.

Section S7. Cryogenic Scanning Transmission Electron Microscopy (Cryo-STEM) and Cryogenic Electron Energy Loss Spectroscopy (Cryo-EELS)

Cryogenic condition is inevitable in the electron microscopy study of sodium with intrinsic high chemical reactivity and low thermal stability to avoid beam damage. This method was only used previously by Sun et al.¹² to probe the SEI growth on sodium in an ionic liquid -based electrolyte, and further by Han et al.¹³ to study the effect of FEC additive on the SEI composition on sodium in carbonate-based electrolyte.

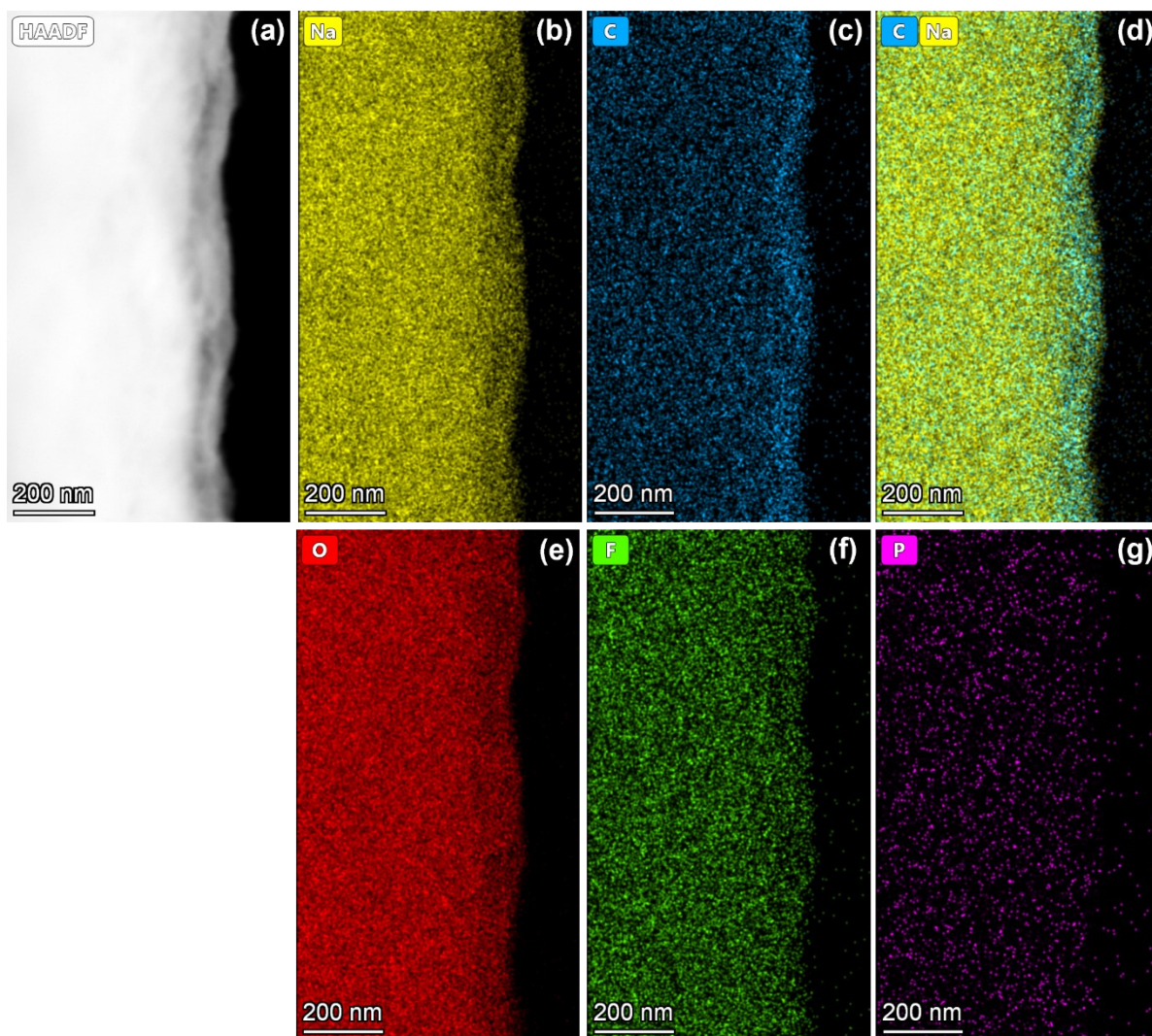


Figure S19. The EDS elemental mapping on the stripped sodium in 1M NaPF₆ in DME. (a) HAADF image, and elemental composition scans in (b) Na, (c) C, (d) overlaid of Na and C, (e) O, (f) F, and (g) P regions. The sodium was plated at 0.5 mA/cm² for 1 mAh/cm² on TEM grid at 180 kPa uniaxial pressure and stripped to 1V at 0.5 mA/cm².

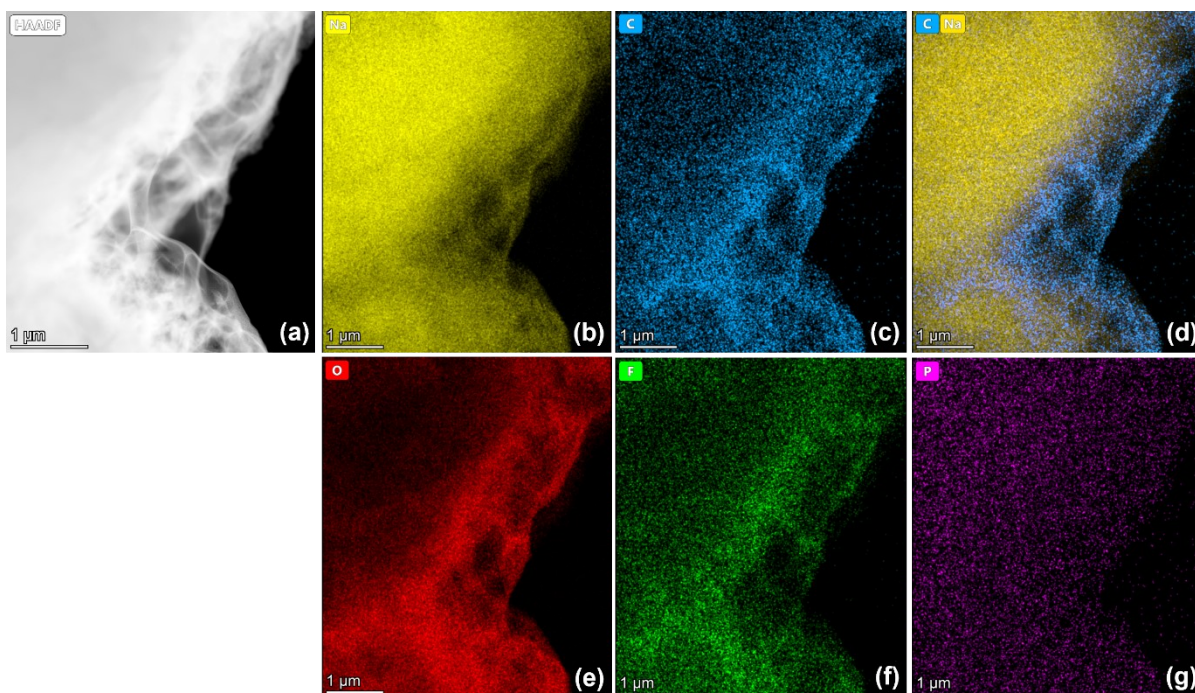


Figure S20. The EDS elemental mapping on the stripped sodium in 1M NaPF₆ in EC:DMC (1:1). (a) HAADF image, and elemental composition scans in (b) Na, (c) C, (d) overlaid of Na and C, (e) O, (f) F, and (g) P regions. The sodium was plated at 0.5 mA/cm² for 1 mAh/cm² on TEM grid at 250 kPa uniaxial pressure and stripped to 1V at 0.5 mA/cm².

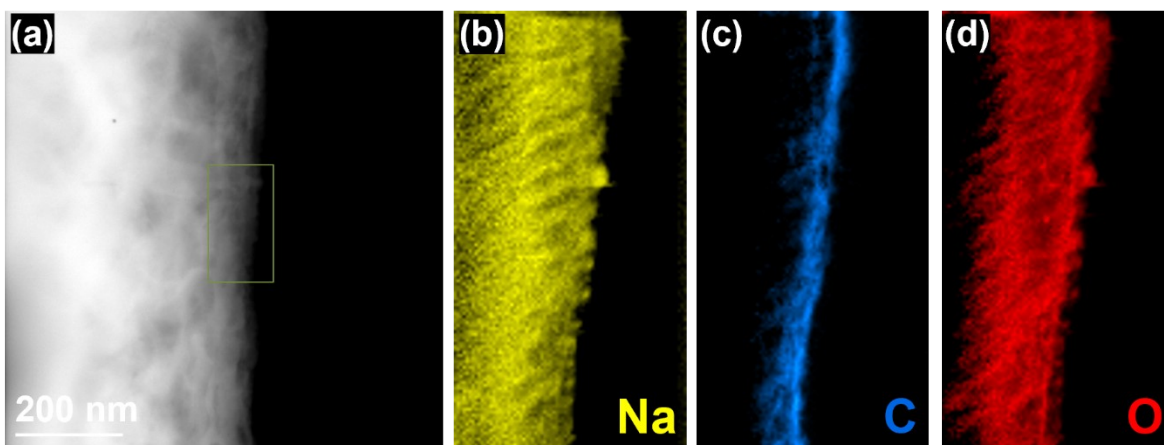


Figure S21. (a) The cryo-EELS elemental mapping in (b) Na, (c) C, and (d) O regions. The samples are stripped sodium in 1M NaPF₆ in DME. The sodium was plated at 0.5 mA/cm² for 1 mAh/cm² on TEM grid at 180 kPa uniaxial pressure and stripped to 1V at 0.5 mA/cm².

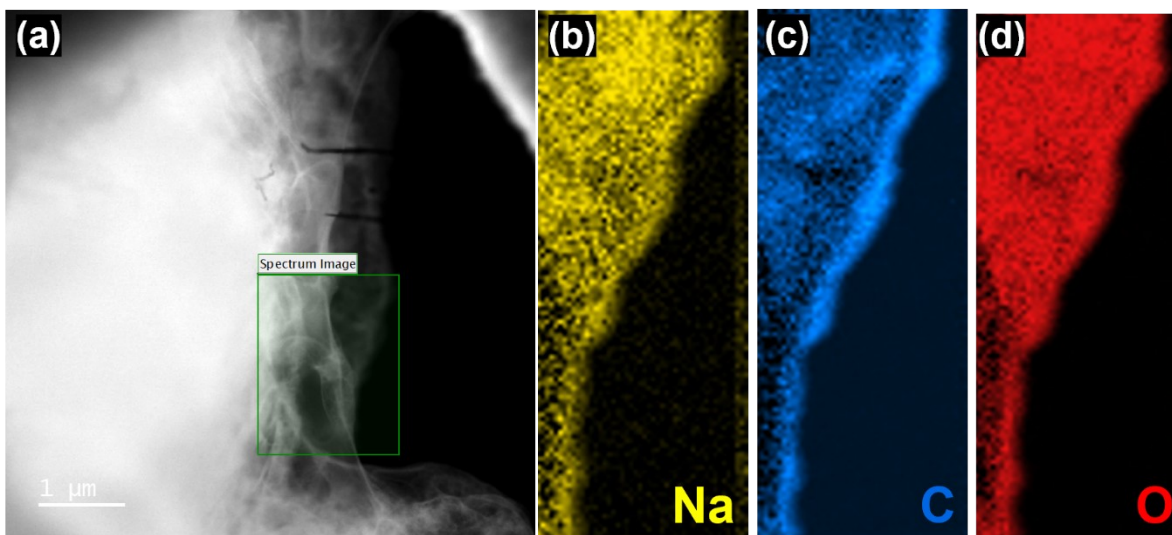


Figure S22. (a) The cryo-EELS elemental mapping in (b) Na, (c) C, and (d) O regions. The samples are stripped sodium in 1M NaPF₆ in EC:DMC (1:1). The sodium was plated at 0.5 mA/cm² for 1 mAh/cm² on TEM grid at 250 kPa uniaxial pressure and stripped to 1V at 0.5 mA/cm².

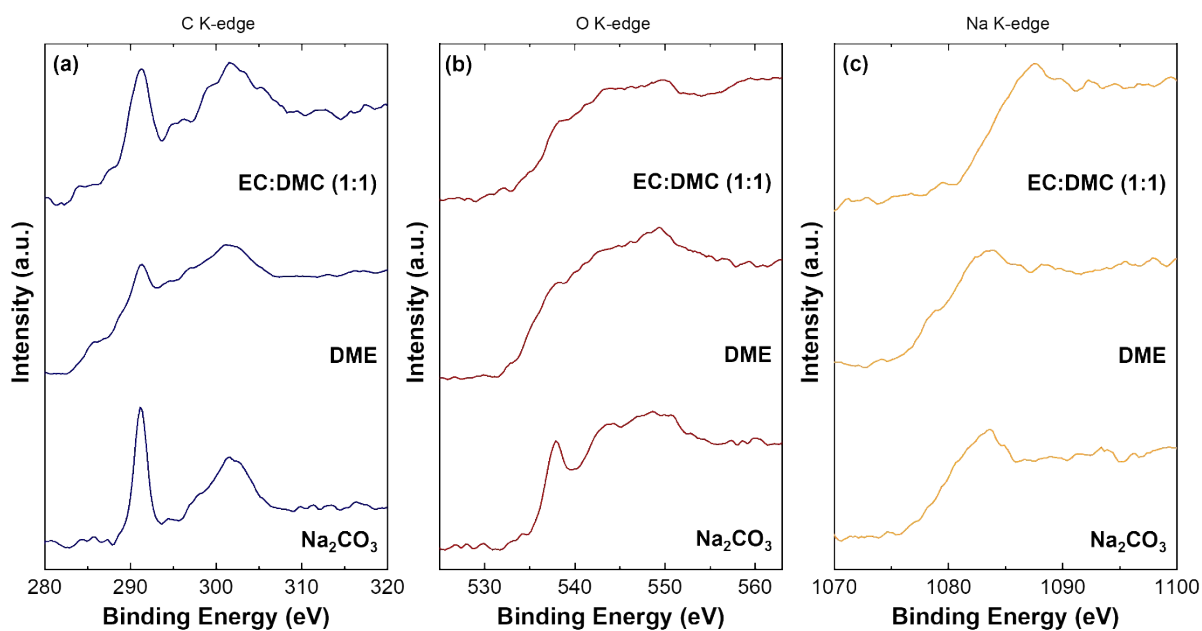


Figure S23. The cryo-EELS spectra of SEI structures of the both electrolytes in (a) C K-edge, (b) O K-edge, and (c) Na K-edge regions, compared to standard Na₂CO₃ powder.

Section S8. Electrochemical Performance – Ether-based Electrolyte

Table S3. Coin-cell testing specifications – Sodium-ion battery using sodium metal anode.

Coin Cell Specifications	
Cell type	CR2032
Cathode active material	NaCrO ₂ – 80wt%
Binder	PVDF – 10wt%
Conductive Agent	Super C65 – 10wt%
Counter electrode	Controlled amount of electroplated sodium
Separator	<u>Celgard 2325</u>
Electrolyte	1M NaPF ₆ in DME
Electrolyte amount	50 μ L
Coin cell setup	0.5 mm thick SS spacer and one spring at the cathode side 0.5 mm thick SS space at the anode side
Voltage range	2-3.6 V
Active material loading	10-15 mg/cm ²
Applied current density	C/3 (based on 120 <u>mAh/g</u> theoretical capacity)

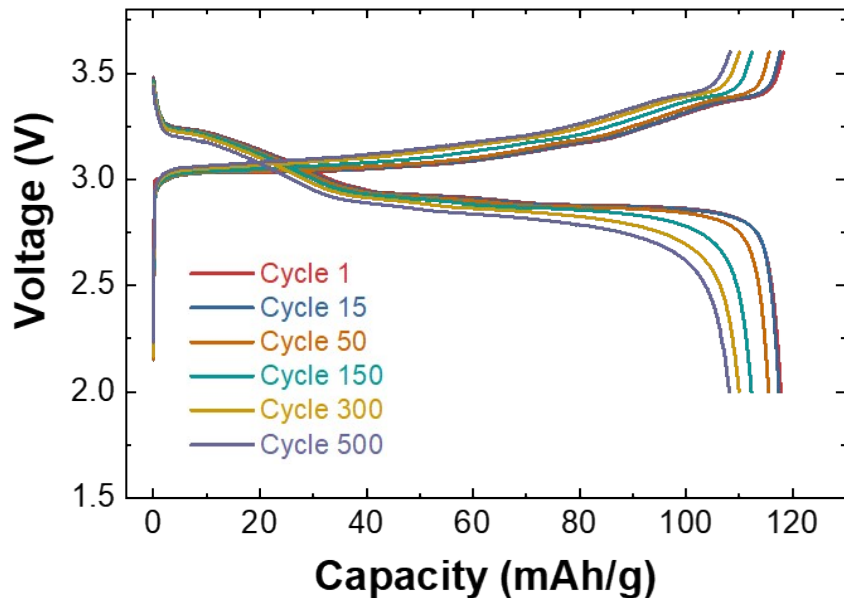


Figure S24. The voltage profiles of the cell consisting of controlled electroplated sodium as the anode, NaCrO_2 as the cathode, and 1M NaPF_6 in DME. This was run at the rate of 2C (considering 120 mAh/g as the total capacity). This data corresponds to the data shown in **Figure 5a**.

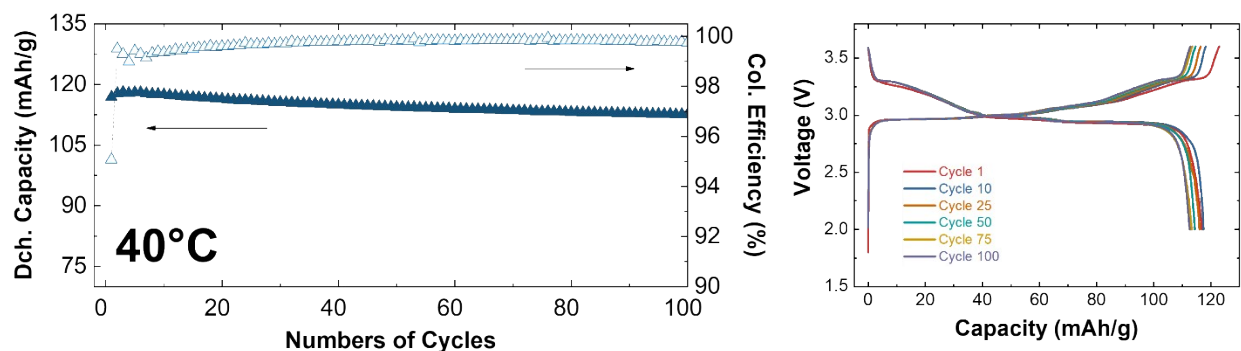


Figure S25. (a) The discharge capacity (mAh/g) and coulombic efficiency (%) versus the numbers of cycles, and **(b)** the voltage profiles of the cell. The cell consists of controlled electroplated sodium as the anode, NaCrO_2 as the cathode, and 1M NaPF_6 in DME. This was run at the rate of $\text{C}/3$ and 40°C (considering 120 mAh/g as the total capacity).

Section S9. Self-Discharge Measurement

The rate of self-discharge recovery was evaluated using the protocol reported by Idaho National Laboratory as a battery test manual¹⁴. Multiple cells were assembled and run under C/3 for the first cycle at room-temperature. The cells stopped in the following second discharge at half of energy density and rested at open circuit condition (disconnected from any device). The cells continued to be discharged separately after different resting times at C/3. This procedure is shown in **Figure S26**.

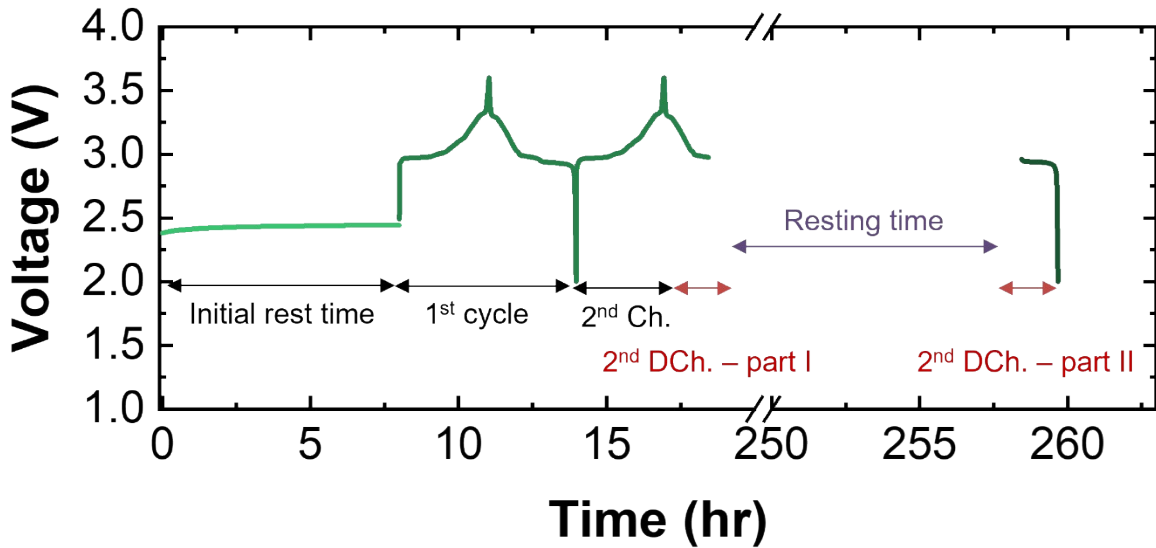


Figure S26. The self-discharge protocol following the Idaho National Laboratory report.

The difference between the energy obtained prior to the test and during the test is considered to be the energy loss reflecting self-discharge during the stand period as shown in Equation 1:

$$\text{Self-Discharge} = \frac{Wh_C \frac{1}{3} \text{ before test} - (Wh_{\text{part 1}} + Wh_{\text{part 2}})}{Wh_C \frac{1}{3} \text{ before test}} \times 100\% \quad (\text{Eq. 2})$$

Section S10. Electrochemical Performance – Carbonate-based Electrolyte

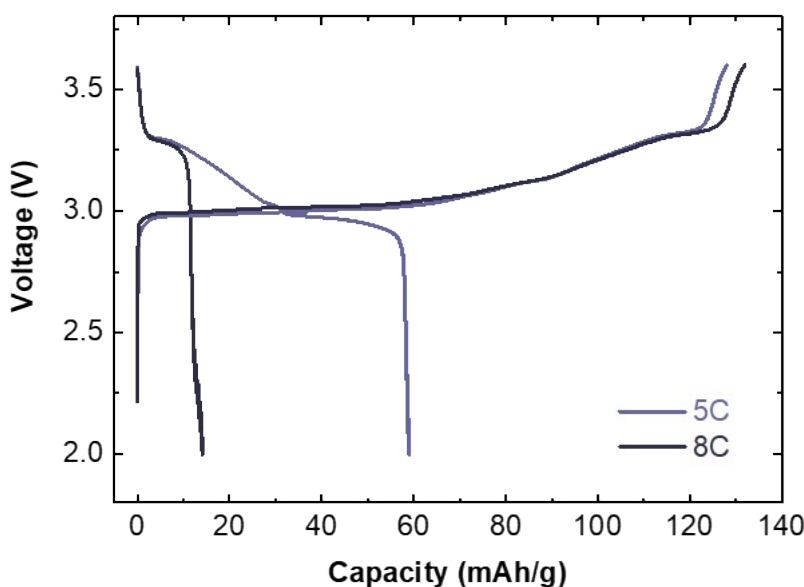


Figure S27. The electrochemical performance of the cell consisting of electroplated sodium as the anode, NaCrO_2 as the cathode (12.8 mg/cm^2), and 1M NaPF_6 in EC:DMC (1:1) as the electrolyte. The cells have controlled 100% excess of sodium inventory. The data shows the first cycle voltage profiles of cell at different C rates of 5C and 8C.

References:

- (1) Fang, C.; Wang, X.; Meng, Y. S. Key Issues Hindering a Practical Lithium-Metal Anode. *Trends Chem.* **2019**, *1* (2), 152–158. <https://doi.org/10.1016/j.trechm.2019.02.015>.
- (2) Fang, C.; Li, J.; Zhang, M.; Zhang, Y.; Yang, F.; Lee, J. Z.; Lee, M. H.; Alvarado, J.; Schroeder, M. A.; Yang, Y.; Lu, B.; Williams, N.; Ceja, M.; Yang, L.; Cai, M.; Gu, J.; Xu, K.; Wang, X.; Meng, Y. S. Quantifying Inactive Lithium in Lithium Metal Batteries. *Nature* **2019**, *572* (7770), 511–515. <https://doi.org/10.1038/s41586-019-1481-z>.
- (3) Carmichael, R. S. *Practical Handbook of Physical Properties of Rocks and Minerals*; CRC Press, 1988.
- (4) Department of Energy, U. *Reaction of Aluminum with Water to Produce Hydrogen, A*

Study of Issues Related to the Use of Aluminum for On-Board Vehicular Hydrogen Storage; 2008.

- (5) Rudola, A.; Rennie, A. J. R.; Heap, R.; Meysami, S. S.; Lowbridge, A.; Mazzali, F.; Sayers, R.; Wright, C. J.; Barker, J. Commercialisation of High Energy Density Sodium-Ion Batteries: Faradion's Journey and Outlook. *J. Mater. Chem. A* **2021**, *9* (13), 8279–8302. <https://doi.org/10.1039/d1ta00376c>.
- (6) Shakourian-fard, M.; Kamath, G.; Smith, K.; Xiong, H.; Sankaranarayanan, S. K. R. S. Trends in Na-Ion Solvation with Alkyl-Carbonate Electrolytes for Sodium-Ion Batteries : Insights from First-Principles Calculations. **2015**. <https://doi.org/10.1021/acs.jpcc.5b04706>.
- (7) Ponrouch, A.; Marchante, E.; Courty, M.; Tarascon, J. M.; Palacín, M. R. In Search of an Optimized Electrolyte for Na-Ion Batteries. *Energy Environ. Sci.* **2012**, *5* (9), 8572–8583. <https://doi.org/10.1039/c2ee22258b>.
- (8) Lin, Z.; Xia, Q.; Wang, W.; Li, W.; Chou, S. Recent Research Progresses in Ether- and Ester-based Electrolytes for Sodium-ion Batteries. *InfoMat* **2019**, *1* (3), 376–389. <https://doi.org/10.1002/inf2.12023>.
- (9) Xu, K. Electrolytes and Interphases in Li-Ion Batteries and Beyond. *Chem. Rev.* **2014**, *114* (23), 11503–11618. <https://doi.org/10.1021/cr500003w>.
- (10) Doux, J. M.; Yang, Y.; Tan, D. H. S.; Nguyen, H.; Wu, E. A.; Wang, X.; Banerjee, A.; Meng, Y. S. Pressure Effects on Sulfide Electrolytes for All Solid-State Batteries. *J. Mater. Chem. A* **2020**, *8* (10), 5049–5055. <https://doi.org/10.1039/c9ta12889a>.
- (11) Lu, B.; Bao, W.; Yao, W.; Doux, J.-M.; Fang, C.; Meng, Y. S. Editors' Choice—Methods—Pressure Control Apparatus for Lithium Metal Batteries. *J. Electrochem. Soc.* **2022**, *169* (7), 070537. <https://doi.org/10.1149/1945-7111/ac834c>.
- (12) Sun, H.; Zhu, G.; Xu, X.; Liao, M.; Li, Y. Y.; Angell, M.; Gu, M.; Zhu, Y.; Hung, W. H.; Li, J.; Kuang, Y.; Meng, Y.; Lin, M. C.; Peng, H.; Dai, H. A Safe and Non-Flammable Sodium Metal Battery Based on an Ionic Liquid Electrolyte. *Nat. Commun.* **2019**, *10* (1), 1–11. <https://doi.org/10.1038/s41467-019-11102-2>.
- (13) Han, B.; Zou, Y.; Zhang, Z.; Yang, X.; Shi, X.; Meng, H.; Wang, H.; Xu, K.; Deng, Y.; Gu, M. Probing the Na Metal Solid Electrolyte Interphase via Cryo-Transmission Electron Microscopy. *Nat. Commun.* **2021**, *12* (1), 3066. <https://doi.org/10.1038/s41467-021-23368-6>.
- (14) Christopherson, J. P. *Battery Test Manual for Plug-In Hybrid Electric Vehicles*; 2015.